Villalobos, J., H. J. McDermott, P. McNeill, A. Golod, V. Rathi, S. Bauquier, and J. B. Fallon. 2020. Slim electrodes for improved targeting in deep brain stimulation. *Journal of Neural Engineering*. **17**: 026008.

doi: 10.1088/1741-2552/ab7a51

Slim electrodes for improved targeting in deep brain stimulation

To cite this article before publication: Joel Villalobos *et al* 2020 *J. Neural Eng.* in press https://doi.org/10.1088/1741-2552/ab7a51

Slim electrodes for improved targeting in Deep Brain Stimulation

Joel Villalobos[1], Hugh J. McDermott[1,2], Peter McNeill[3], Aharon Golod[1], Vivek Rathi[3], Sébastien H. Bauquier[4], and James B. Fallon[1,2]

1 Bionics Institute, East Melbourne, Australia

2 Medical Bionics Department, The University of Melbourne, VIC 3002, Australia

3 St Vincent's Hospital Melbourne, Fitzroy, VIC 3065, Australia

4 Translational Research and Animal Clinical Trials (TRACTs), Faculty of Veterinary and Agricultural Sciences, The University of Melbourne, Werribee, VIC 3030, Australia

Correspondence:

Joel Villalobos
Bionics Institute
jvillalobos@bionicsinstitute.org
384-388 Albert St
East Melbourne, VIC 3002
Australia

Abstract

Objective: The efficacy of deep brain stimulation can be limited by factors including poor selectivity of stimulation, targeting error, and complications related to implant reliability and stability. We aimed to improve surgical outcomes by evaluating electrode leads with smaller diameter electrode and microelectrodes incorporated which can be used for assisting targeting.

Approach: Electrode arrays were constructed with two different diameters of 0.65 mm and the standard 1.3 mm. Micro-electrodes were incorporated into the slim electrode arrays for recording spiking neural activity. Arrays were bilaterally implanted into the medial geniculate body (MGB) in nine anaesthetised cats for 24–40 hours using stereotactic techniques. Recordings of auditory evoked field potentials and multi-unit activity

were obtained at 1 mm intervals along the electrode insertion track. Insertion trauma was evaluated histologically.

Main results: Evoked auditory field potentials were recorded from ring and micro-electrodes in the vicinity of the medial geniculate body. Spiking activity was recorded from 81% of the microelectrodes approaching the MGB. Histological examination showed localized surgical trauma along the implant. The extent of haemorrhage surrounding the track was measured and found to be significantly reduced with the miniature slim electrodes (541±455 µm vs. 827±647 µm; $P < 0.001$). Scoring of the trauma, focusing on tissue disruption, haemorrhage, oedema of glial parenchyma and pyknosis, revealed a significantly lower trauma score for the slim electrodes ($P < 0.0001$).

Significance: The slim electrodes reduced the extent of acute trauma, while still providing adequate electrode impedance for both stimulating and recording, and providing the option to target stimulate smaller volumes of tissue. The incorporation of microelectrodes into the electrode array may allow for a simplified, single-step surgical approach where confirmatory micro-targeting is done with the same lead used for permanent implantation.

1. Introduction

Deep Brain Stimulation (DBS) is a widely used therapy based on electrical stimulation of the central nervous system. It is indicated for treating symptoms of Parkinson's disease [1] and it has been used to treat a wide range of neurological conditions [2, 3]. More than 100,000 patients have been implanted with a DBS device, primarily people living with Parkinson's disease that have become less responsive to Levodopa over time [4]. However, there is growing evidence that DBS can be beneficial in earlier stages of the disease [5]. DBS therapy can alleviate the motor symptoms that most affect the quality of life [6], although efficacy is significantly affected by factors including poor selectivity of stimulation, targeting errors, and the natural variation of symptoms over time [7, 8].

The DBS implantation procedure is relatively safe. Hardware-related complications however are common and reported in 8–19% of cases [9-11]. These include lead fracture, infection, stimulator problems, extension cable faults, and lead migration. The most serious risk is intracranial haemorrhage, which has been reported with an occurrence of 1-4% [12-14]. The physical configuration of the DBS hardware has remained largely unchanged for over two decades. The brain-penetrating electrode lead, in particular, has generally maintained a consistent diameter of around 1.3 mm. Recent innovations on leads have focused on segmenting the ring electrodes to enable steering the stimulation current field [15-17] or recording neural potentials [18]. This constancy in lead diameter is surprising given that thinner electrode leads have been used for animal studies with diameters varying from 0.08–0.2 mm [19] to 1.1 mm [20].

It has been proposed that reducing the overall size of the DBS hardware would be beneficial and could decrease the rate of complications [21]. However, a reduction in lead diameter could adversely affect the accuracy of electrode placement, since current surgical techniques have targeting errors of only 1.2±0.6 mm using a full frame (or 2.5±1.4 mm for frameless procedures) [22] when targeting the basal ganglia. These errors are due to a mixture of inherent inaccuracies in the imaging techniques that fuse preoperative magnetic resonance imaging with x-ray computed tomography, as well as brain shift during surgery (from gravity, brain deformation, and cerebrospinal fluid loss) [23, 24]. Accuracy is often improved by a separate step of intraoperative targeting verification, typically through microelectrode recordings[25, 26], although implantable radiopaque guide tubes [27] for imaging guidance (in two different surgery stages) have been proposed as an alternative.

With the aim to simplify the surgical implantation, we proposed using thinner electrode leads with incorporated microelectrodes. This would achieve a single-step surgical insertion with targeting verification using the lead intended for permanent implantation (

Figure 1). This study evaluated the effect of using the slim electrode lead with microelectrodes, which is half the diameter of standard leads (e.g. Medtronic Lead 3387) and similar to targeting electrodes (e.g. FHC STarFix microelectrodes). Preliminary results of this comparison were presented previously [28]. In the report below we describe the trauma from acute *in vivo* implantation of the electrode leads, with a comparison of the accuracy of the insertion trajectory using a transparent gel model of brain tissue. The electrode leads incorporate microelectrodes to enable localised recording of high frequency brain potentials [29, 30], but instead of constructing the lead with a thin film substrate [31], a soft polymer substrate was used to maintain the flexibility of typical DBS leads.

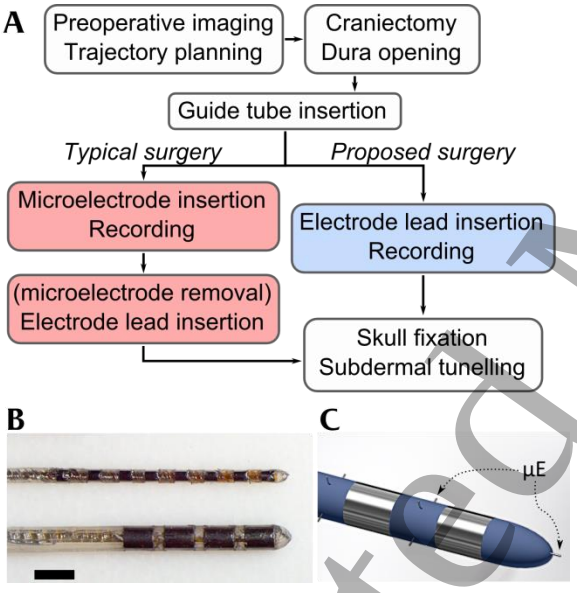

Figure 1. (A) With incorporated microelectrodes in a DBS lead, the critical surgical insertion procedure can be simplified to a single step. (B) The slim electrode lead (ø 0.65 µm) is ¼ of the volume of standard DBS leads (ø 1.3 mm). Scale bar is 2 mm. (C) The electrode lead incorporates microelectrodes (µE) at the tip and sides to perform neural recordings.

2. Methods

2.1. Electrode Leads and Cannulas

The Deep Brain Stimulation electrodes were assembled in-house using platinum rings (Johnson Matthey Medical) in a silicone rubber substrate. There were two electrode lead diameters: 0.65 mm and 1.3 mm. The smaller electrode lead contained 8 electrodes of 0.65 mm diameter and 0.65 mm length, at a 1.5 mm pitch. Wires of 25µm diameter (Pt-Ir alloy) protruded from the substrate to become microelectrodes for neural

recording. There were 2 microelectrodes at the tip, for redundancy, and up to three microelectrodes on the side, interspaced with the rings (

Figure 1C). The larger lead had 4 electrodes of 1.3 mm diameter and 1.5 mm length, at a 3 mm pitch, to mimic standard DBS electrodes. The substrate was injection-moulded with silicone rubber (MED4840; Nusil Technology). The electrode lead was hollow and contained a stylet made with thin tungsten wire (Goodfellow). Electrode impedances in vivo were measured with a Pt reference and large Pt counter-electrode, using a potentiostat (Solartron).

DBS electrodes are normally implanted stereotaxically into the desired target using metal cannulas that stop short (e.g. 10 mm) of the target. A custom cannula for the slim electrode lead was made using stainless steel tube. The outer diameter of the cannula was 1.1 mm for the distal 80 mm that penetrated the brain, and 1.8 mm for the rest of the length to fit into standard stereotaxic guidance equipment. The cannula used for the 1.3 mm implant was from a microtargeting tube insertion set (FHC Inc). The cannulas had a solid stiffening rod used for the initial insertion into the tissue, which was subsequently removed to insert the electrode lead.

2.2. In vivo acute implantation

The DBS electrodes were implanted acutely under anaesthesia in 9 adult cats (3.1–6.2 kg) for a duration of 24 to 40 hours. Electrode leads of both dimensions were implanted into the thalamus in each hemisphere. The protocols were approved by the Animal Research Ethics Committee of the Royal Victorian Eye and Ear Hospital and were compliant with: the "Australian code of practice for the care and use of animals for scientific purposes" (7th edition 2004), the Australian "Prevention of cruelty to animals act" (1986), and the "principles of laboratory animal care" (NIH publication 85-23, revision 1985).

2.2.1. Anaesthesia

After the cats were premedicated with intramuscular medetomidine (0.015 mg/kg), ketamine (10 mg/kg) and methadone (0.5 mg/kg), a 22 G catheter was placed in a cephalic vein. General anaesthesia was then induced with intravenous administration of propofol to effect (0–2 mg/kg) and the trachea of the cats was intubated with a cuffed endotracheal tube. Anaesthesia was maintained with methadone intravenous constant rate infusion (0.05 mg/kg/h) and propofol intravenous infusion to effect (0.05–0.2 mg/kg). Throughout the anaesthesia, 100% oxygen was provided and the cats were mechanically ventilated to maintain normocapnia. A multi-parametric anaesthesia monitor was used to monitor electrocardiogram, heart rate, mean arterial

blood pressures, respiratory rate, partial pressure of end-tidal carbon dioxide ($PETCO_2$), oxygen haemoglobin saturation (by pulse oximetry [SpO_2]) and temperature.

2.2.2. Surgery

The 0.65 mm diameter electrode lead was stereotaxically inserted towards the medial geniculate body of the thalamus, and the 1.3 mm diameter electrode lead was implanted in a parallel trajectory, 4 mm rostral. The animal's head was mounted in the stereotaxic frame (David Kopf Instruments, Tujunga CA, USA) using hollow ear-bars to permit auditory stimulation. The coordinates were calculated from a brain atlas [32], with reference to the interaural line and midsagittal plane. A cannula was inserted to 6 mm above target (half of insertion depth) and the electrode leads inserted through it and advanced slowly with a micromanipulator (STar Drive; FHC Inc, Bowdoin ME, USA) mounted with a custom-built adaptor. The electrode lead was fixed in place, typically at 2 mm past the calculated target, using bone cement to fill the 2–3 mm diameter craniotomy.

2.2.3. Neural recordings

Recordings of brain activity were obtained at every 1 mm of depth (or more frequently when spiking activity was detected) using a multichannel recording system (Blackrock Microsystems, Salt Lake City UT, USA). The signal from the microelectrode at the tip was played on a speaker as the implant was advanced, similar to functional neurosurgery in DBS patients. Once the implant was fixed, recordings were repeated every few hours for the course of the implantation period. The recordings were performed either in silence or with an auditory stimulus intended to activate the medial geniculate body. The auditory stimuli consisted of trains of 2 ms noise bursts at 25 Hz presented for 2 seconds alternated with 2 seconds of silence. Evoked potentials were analysed offline from both macro electrodes and microelectrodes. Spontaneous multi-unit activity in the form of spikes was filtered (0.5-2 kHz) and obtained from the microelectrode recordings, using recordings where no auditory stimuli were presented. Spikes events were defined as signal incursions beyond 4 times the root-mean-square of voltage magnitude, which were counted and divided by the length of the recording (typically 60 seconds) to obtain the spike per second rate.

The location of each electrode was measured from histological slides, where the track offset and the final depth were measured from the centre of the MGB. To assess the spread of the evoked potential or spatial

decay of the signal, the slope of a linear fit was calculated using the evoked potential amplitude vs distance to MGB in all the electrodes that had recordings on at least 3 depths.

2.2.4. Histology

At the end of the experiment, the animals were euthanized with an overdose of sodium pentobarbitone (150 mg/kg; Lethabarb) and perfused intracardially with warm saline (37 °C) followed by neutral buffered formalin (4 °C). The collected brains were postfixed in neutral buffered formalin for 24–48 h. The paraffin embedded tissue was sectioned (5 μm) and stained with haematoxylin and eosin (H&E). Selected slides containing the electrode tracks were stained with a terminal d-UTP nick-end labelling (TUNEL) assay using a green fluorescent protein marker and with 4′,6-diamidino-2-phenylindole (DAPI) for background.

Representative sections were chosen from each implant track: the best section showing a centred region of the deep implant track with the least amount of histological artefact. Assessment of the surgical trauma to the brain tissue, related to the injury from electrode insertion, was carried out keeping in mind the extent of tissue disruption, haemorrhage, oedema of the glial parenchyma, and the extent of neuronal injury (pyknosis) in parenchyma close to the tract. A cumulative score ranging from 0-10 was given by the pathologist (V Rathi) and implantable device specialist (J Villalobos) based on the factors mentioned above; 0 being no damage and 10 being severe damage. The scores from the two assessors were averaged for each slide and the correlation checked for consistency. While the assessors were blinded during scoring of histological slides, it was evident when the track was from a standard or slim implant from anatomy and width of the track.

As an independent parallel assessment, a script programmed in ImageJ software (NIH) measured the area of haemorrhage adjacent to the track from the microphotographs where the track was visible. Haemorrhage was defined as the area where the image colour reached a 95% red threshold, after normalising the background to pure white. The measured area was divided by the length of visible track to give a measure of extent of haemorrhage (with linear units), similar to an even thickness around the track. The track haemorrhage extent was compared within hemispheres to account for differences in physiological response, duration of experiment and potential confounding with adjacent track.

Apoptotic cell counts on the representative slides with TUNEL staining were done from the digitized 20x microphotographs (Zeiss AxioImager) using custom ImageJ scripts. The scripts isolated a region of interest

extending 300 µm from the electrode track, and counted the total cell nuclei in the blue DAPI channel and the TUNEL positive nuclei in the green channel.

2.3. Lead deflection testing in gel model

The slim and standard size electrode leads were inserted into blocks of agarose gel to measure trajectory deviation and insertion force. This enabled direct observation of the trajectory which is concealed in vivo by the tissue. There were 6 electrode leads of each type. A 30 mm × 30 mm × 30 mm gel block with 0.6% agarose was used as a mechanical model of brain tissue [33]. Each insertion included inserting and fixing the cannula into a fresh area of agar gel and removing the cannula stiffening rod. Subsequently the implants were inserted through the cannula and advanced at a rate of 2 mm/s to project 10 mm from the cannula. The implant was pushed into the gel by a force gauge (M5-05; Mark 10) attached to a micromanipulator (MP-285; Sutter Instrument). The trajectory deviations were measured from images taken with close-up cameras (Digitech 5MP) on two orthogonal planes, which were analysed in ImageJ software (NIH).

2.4. Statistical analysis

The main results are reported below as means ± standard deviation. Comparisons between the slim and standard sized implant for histological trauma quantification were done using paired t-tests, or non-parametric (Mann-Whitney) tests for subjective trauma scoring. In the case of implant insertions into gel, where multiple insertions were done with each implant, comparisons were made with a General Linear Model using the implant diameter as fixed factor and specific implant as random factor.

3. Results

3.1. In vivo electrode impedance

Electrode impedance was measured in a subset of electrodes after full insertion into brain tissue. The in vivo impedance magnitude of the standard sized DBS electrodes (n = 10) was 1.2±0.3 kΩ (at 1 kHz). The impedance of the slim stimulating electrodes (n = 20) was higher at 2.0±0.6 kΩ, corresponding to a decrease in geometric surface area from 7.1 mm^2 to 1.3 mm^2. The microelectrodes (n = 29), made of Pt|Ir wire protruding from the substrate, had an impedance magnitude in vivo of 294±174 kΩ.

3.2. Neural Recordings

Brain activity was recorded using the ring electrodes and microelectrodes from the slim electrode leads. These were inserted towards the MGB while recordings were made at 1 mm steps. Typically, in the subset of electrodes that approached the MGB, the amplitude of the auditory evoked potential increased with advancing depth, to reach a maximum of 4.1±2.3 mV for the ring electrodes (20 out of 32) and 4.4±1.9 mV for the microelectrodes (30 of 41) (Figure 2). Figure 2A shows the increase in evoked potential amplitude with proximity to the MGB observed in both ring and microelectrodes. The peak amplitude of the evoked potential was similar in microelectrodes and the ring electrodes (Figure 2B), as well as the decay rate (slope of linear fit) of the signal with distance away from the MGB (Figure 2C), indicating an alignment in the volumetric spread of the signal which was not affected by electrode size. The evoked potential observed in both types of electrodes had a strong correlation to the distance from MGB (Figure 2D).

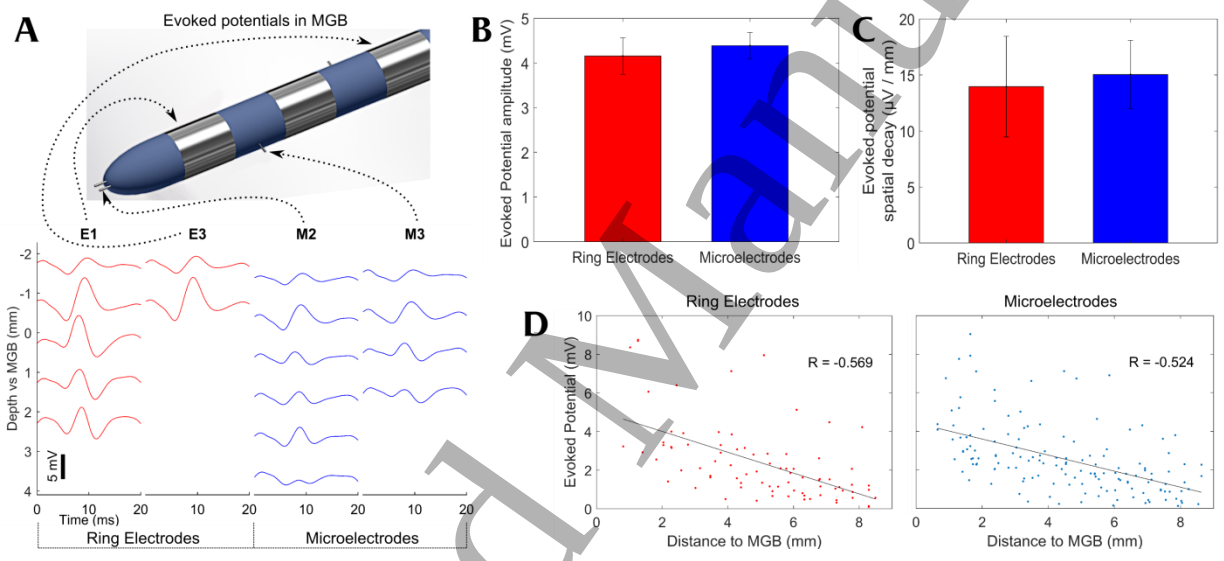

Figure 2. Auditory evoked potentials recorded from electrodes at (A) advancing depths towards cat medial geniculate body (auditory thalamus) showed a change in signal amplitude with proximity to the MGB (signals shown up to maximum depth for each electrode). Red traces recorded from rings and blue traces from microelectrodes (B) The maximum evoked potential signal amplitude was similar for ring macro-electrodes (n = 20) and microelectrodes (n = 30), and (C) both showed a similar spatial attenuation pattern. (D) The amplitude of the evoked potential correlated with the histologically-measured distance to MGB.

The microelectrodes were used to record and listen for high frequency spiking activity at advancing depths. Figure 3 shows an example of spike rates changes over penetration distance. The amplified signals from microelectrodes at the tip were played through a speaker during insertion, without auditory stimuli, in a

similar fashion to microtargeting during DBS surgery for movement disorders albeit on a different target. Changes in spiking activity with depth were identified in 17 of the 30 microelectrodes which were close to the MGB. After histological tracing of the electrode track to identify electrodes reaching the MGB, it was confirmed that 5 of the 7 microelectrodes at the tip and 8 of the 9 microelectrodes on the implant side showed increased spiking activity with proximity to the MGB. The spiking activity observed in microelectrodes on the side of the implant, usually increased hours after implantation (Figure 3C).

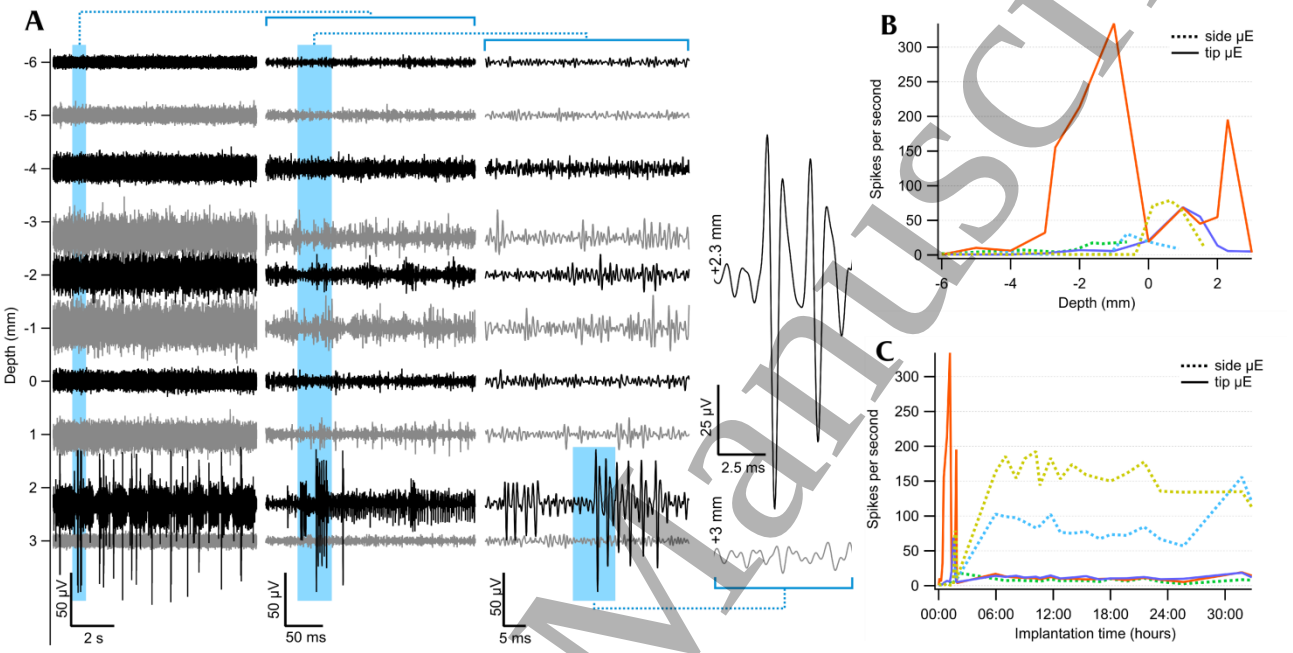

Figure 3. Spiking activity in cat thalamus using microelectrodes incorporated in the slim electrode lead. (A) Left plot shows filtered recordings from one tip microelectrode at increasing depth. The second, third and fourth panels show increased time magnification (corresponding to blue areas). (B) Spike rate of 5 different microelectrodes vs. implant depth, where solid lines were the tip electrodes and doted lines were electrodes on the side. (C) Spiking activity evolved hours after implantation. Microelectrodes on the side of the implant (green and blue dotted lines) reliably recorded multiunit activity after recovery from initial surgical insult.

3.3. Surgical Trauma

There were 37 implant tracks from 9 brains. Examination of histological slides of the cerebral tissue surrounding the implantation track showed generally mild penetrating trauma, with focal haemorrhage and oedema extending from the track (Figure 4).

The trauma was scored by an experienced anatomical pathologist (V Rathi) and a researcher experienced with surgical trauma (J Villalobos), with respect to tissue disruption, haemorrhage (Figure 4E), oedema (Figure 4G), and the extent of neuronal injury. Overall, the standard size implant tracks showed a larger extent of trauma, albeit some standard size tracks had only mild haemorrhage and inflammation. The mean trauma score for the slim implant tracks of 2.3±1.0 was significantly lower than the score for the standard implant track 4.7±1.6 (Mann-Whitney $W = 184$, $P < 0.0001$) (Figure 5B). The scores from the two appraisers were highly consistent (mean difference of 0.9±0.8) and correlated (Pearson $R = 0.81$, $P < 0.001$). The range of tissue response was scored in a range from 1 for very mild trauma, 2 (Figure 4F), 4 (Figure 4E), 6 (Figure 4H) or up to 8 for extensive trauma (Figure 4I).

Measurement of the extent of haemorrhage using computer software also showed a higher level of trauma for the standard sized vs. slim electrode tracks. The mean haemorrhage extent for the slim implant tracks was calculated at 541±455 µm, while for the standard tracks it was 827±647 µm (paired t-test: $T = -3.23$; $P = 0.005$). In each implanted brain hemisphere, the standard sized track had between 1.2 and 2.8 times (95% confidence interval) the extent of haemorrhage of the slim track.

The proportion of apoptotic cells surrounding the slim electrode track was significantly lower than for the standard tracks (t-test $T = 3.73$, $P = 0.001$). The TUNEL positive cells around the slim implant tracks (n = 17) (Figure 6) were 14±12% of the total cells whereas around the tracks for standard electrodes (n = 17) these were 31±14%. The range was large and there were tracks of both slim and standard electrodes with minimal TUNEL staining, below 3% (Figure 6C).

There were 2 (out of 18) brain hemispheres where there was an overt intracerebral haemorrhage adjacent to the standard size implant track. These were the only situations where the trauma extended further than 1 mm from the implant track, although the haemorrhage did not join the nearby slim implant tracks. In all cases, there was brain tissue separating the slim track and the standard size track (4 mm distance) which was free from trauma. No overt intracerebral haemorrhages were seen in the region implanted with the slim electrode.

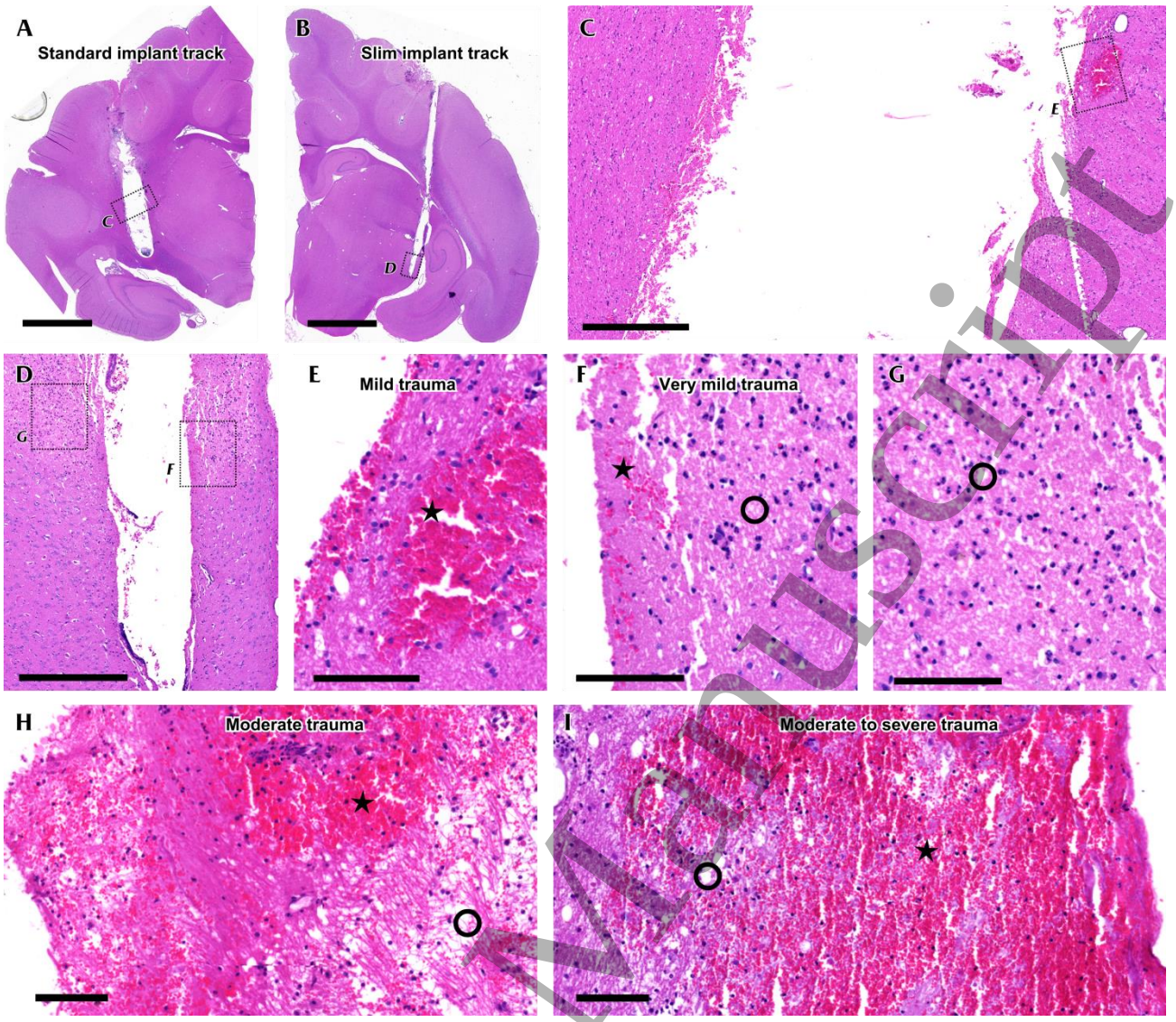

Figure 4. Histological images showing DBS implant tracks of (A, C) standard sized implant, and (B, D) slim implant. There was mild haemorrhage (star) in both standard (E) and slim implant tracks (F) with a small degree of oedema (circle) and inflammation (G). In 5 implant tracks, moderate to severe trauma was observed with either distinct areas of haemorrhage (H) or more extensive regions (I). Trauma scores were 2 for F,G; 4 for E, 6 for H, and 8 for I. H&E stain. Scale bar is 5 mm for A, B; 1 mm for C, D; 100 µm for E, F, G, H, I.

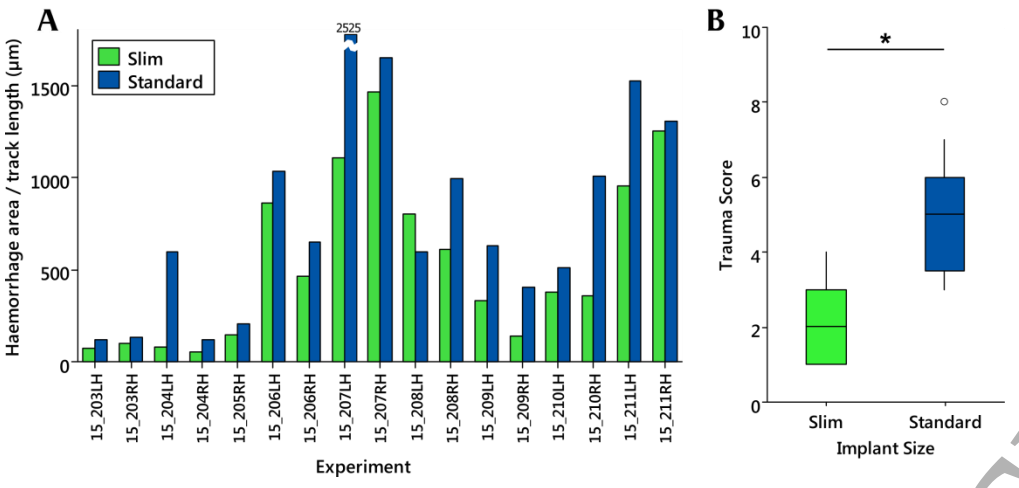

Figure 5. (A) The extent of haemorrhage was generally higher for the standard size implant in each brain hemisphere (paired t-test $P = 0.005$). The left (LH) and right (RH) hemisphere per experiment were treated separately. (B) The qualitative trauma scores were significantly higher for the standard size implants when also considering parenchymal oedema, tissue disruption, and neuronal injury (star shows: $P < 0.001$) (boxes show interquartile range with median line and whiskers show full range).

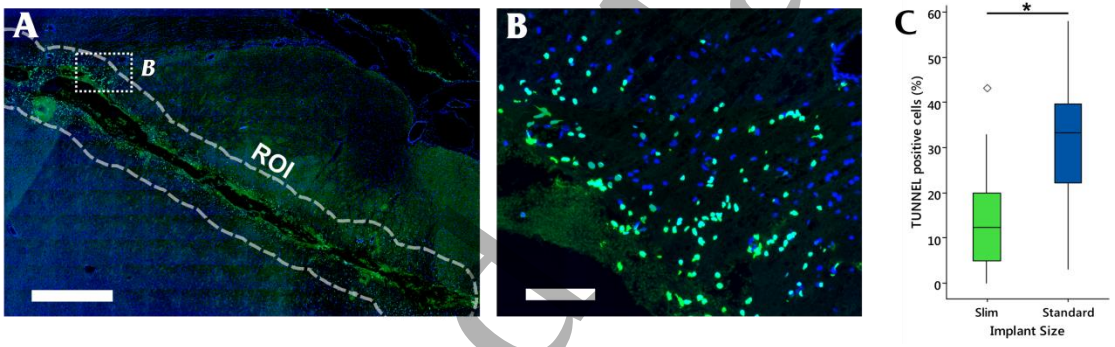

Figure 6. TUNEL staining was used to quantify apoptotic cells. (A, B) The 300 µm of tissue around the electrode track was processed to count the proportion of TUNEL positive cells (green) vs total cells (blue) in the region of interest (ROI). (C) The slim implant produced significantly lower proportion of TUNEL positive cells (n = 17; star shows: $P = 0.001$; boxes show interquartile range with median line and whiskers show full range). Scale bar is 1 mm for A; 100 µm for B.

In 6 of 17 standard sized implant tracks and 3 of 18 slim implant tracks, a region with more extensive trauma was noticeable halfway through the track depth. This depth corresponded with the transition between the cannula and the implant. The location of the damage resembled the bubbles observed during gel insertion tests [28]. These air bubbles formed in gel after withdrawing the filling rod and inserting the electrode lead.

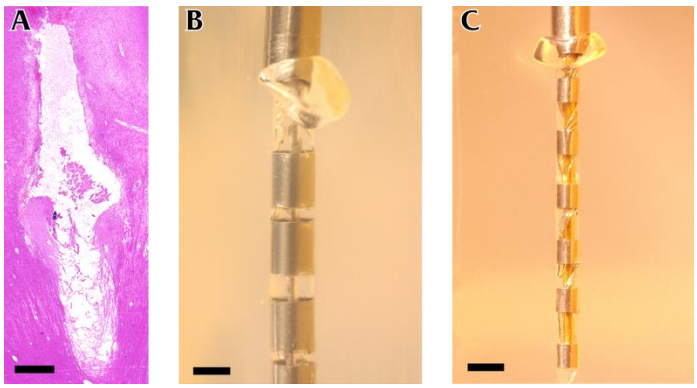

Figure 7. Occasionally, insertion trauma was wider at the transition between cannula and implant. The wide shape and the location of the specific trauma (A) coincides with those of bubble formation observed during insertion of the standard (B) and slim (C) implants into agar gel. Scale bar is 1 mm.

3.4. Implant deflection and insertion forces

The insertion force and trajectory deviation were measured using gel blocks as a model of brain tissue. Using 6 implants of each diameter (slim vs. standard), each implant was inserted 3 times into a fresh portion of gel block through its cannula. As expected, the smaller diameter implants needed lower force for driving into the gel with 43±25 mN, compared with the standard diameter implants at 84±28 mN (ANOVA, $F = 11.10$, $P < 0.001$).

The slim implants were found to have improved targeting accuracy. The absolute deviation from the cannula trajectory was calculated from measurements in two orthogonal images at the full travel of 10 mm. Figure 8 shows that the slim implants had smaller mean deflection at 1.2±0.5° compared to the standard sized implants at 2.4±1.4° (ANOVA, $F = 6.42$, $P = 0.03$).

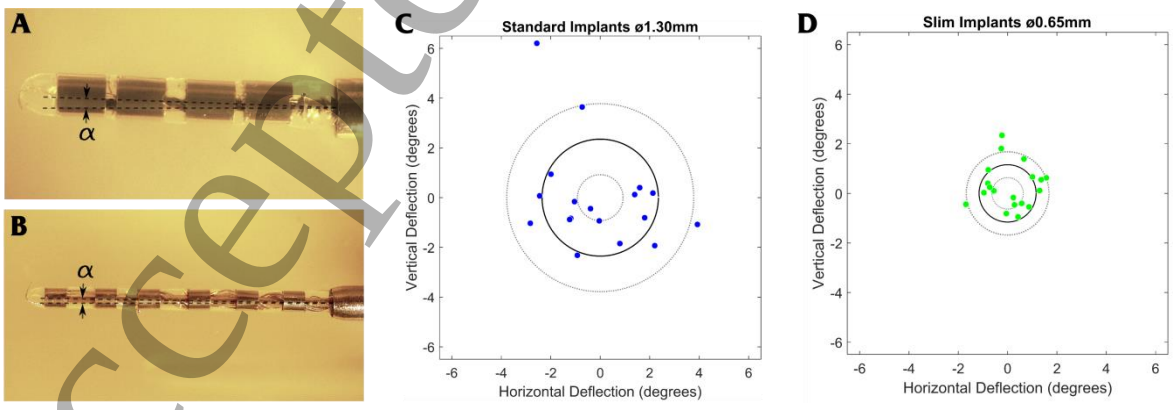

Figure 8. The standard sized (A) implants showed more deviation (C) than the slim implants (B; D) when inserted into 0.6% agarose gel at 2 mm/s. With cameras from the top (A, B) and side, the vertical and

horizontal deflection angles (α) were measured as the implants projected 10 mm from the cannula. Solid lines in plot represent the mean deflection and dotted lines the standard deviation.

4. Discussion

Electrode leads for DBS have a well-established safety record and the technology is considered mature after decades of development on the electrode, stimulator and surgical devices [21]. The findings of this study, however, indicate that there is merit in shrinking the size of the electrode lead since it leads to a significant reduction in trauma and, possibly, an improvement in lead insertion accuracy. Incorporating microelectrodes offers a further improvement to enable a single-insertion-step surgery where the target verification is done with the electrode intended for permanent implantation. Moreover, increasing the density of electrodes [17] facilitates the development of the next generation of DBS systems using closed-loop stimulation.

The result of improved insertion accuracy seen in agar gel insertions was largely unexpected. The deflection from straight lead trajectory must be related to the stiffness of the stylet and the ratio of outer lead diameter versus to internal cannula diameter. The larger leads will always need more slack in this diameter ratio to minimise friction from a larger surface area. But most importantly, we expect that the slim electrode leads will perform with no worse accuracy than the current standard DBS electrodes.

The electrode size used in this study produced a less than 2-fold increase of the in vivo electrochemical impedance. This suggests that providing electrical stimulation at similar charge levels as typical DBS, could increase power requirements and therefore shorten the battery life. However, the smaller electrodes may enable stimulation of smaller volumes of tissue when placement is optimal and consequently the charge required to achieve therapeutic outcomes could be decreased. If larger stimulation volumes are required, to mimic typical DBS stimulation, then pairing two adjacent electrodes would yield similar reach and impedance as a standard sized ring electrode.

The incorporation of microelectrodes into the DBS electrode lead adds significant value to the device by eliminating the need for a two-step surgery, where a first pass uses a microtargeting electrode and a second the DBS electrode lead. The depth patterns of microelectrodes recordings on the implant's tip (Figure 3) resembled those reported in subthalamic targeting during DBS surgery [25], albeit activity spontaneous activity patterns will clearly be different in the MGB. The slim electrode lead presented here is smaller than

the outer diameter of microtargeting electrodes (e.g. FHC), resulting in no extra tissue displacement relative to the microelectrodes used for surgical planning. A one-step surgery where the electrode lead is left in situ when the optimal electrode position has been located, would eliminate the risks of error when positioning the stimulating DBS lead at the same depth as the targeting microelectrode.

A higher density of electrodes on the lead is an active pursuit by DBS electrode manufacturers [2, 17] since the dimensions of typical electrodes (e.g. Medtronic Lead 3387) allow only up to two contacts in small targets like the subthalamic nucleus. The ability to record local field potentials from microelectrodes (as shown in Figure 2) enables placing extra recording channels within the desired target, which could be used for recording biomarkers of interest like beta band activity [34], evoked resonant activity [35] or high frequency oscillations [29].

In this study, the trauma caused specifically by the protruding microelectrodes is confounded with that of the surgical insertion of the slim electrode lead. However, the trauma was significantly lower for the slim electrodes compared with a standard lead. While microelectrodes on the lead have Further investigation is necessary to evaluate if the protruding microelectrodes contribute to the undesired tissue damage.

It should be noted that the slim and standard electrode leads were inserted into different brain regions, since the slim leads with microelectrodes were inserted towards the MGB. The different disposition of brain tissue could have a confounding effect on the amount of haemorrhage quantified, but the quantification of proportion of apoptotic cells labelled with TUNEL would be more robust to the anatomical differences. The overt haemorrhage observed adjacent to 2 standard sized electrode tracks also has to be considered in this context, especially given the stereotaxic targeting was not based on brain imaging which would have allowed trajectory planning to avoid large vessels, as done in human DBS surgery.

This acute histological assessment of the surgical trauma is expected to be more extensive than the chronic foreign body reaction. It is known that standard DBS implants are associated with only a thin glial capsule, as observed postmortem in humans [36, 37] and in minipigs [38]. This comparison of slim electrodes should therefore be extended to chronically implanted animals to verify if the slim leads incorporating microelectrodes are safe for long term use.

Overall, the slim electrode leads provide a safe alternative to the current standard electrode leads and the slim cannula hardware can be assembled to fit on standard DBS surgery equipment. The reduction to a single insertion step by incorporating microelectrodes in the same lead, provides an opportunity to improve current surgical practice without adversely affecting targeting accuracy. Increasing the density of electrodes at the target tissue, with a combination of micro- and ring stimulation electrodes, could result in better control of the tissue targeted by DBS and enable developing technologies for closed-loop DBS in the near future.

5. Acknowledgements

We thank Robert K. Shepherd and Chris Williams for his contributions to implant development and study design; Laura Didier for her contribution to histological analysis; Lisa Cardamone, Catherine Gaunt and Nicole Critch for assistance during experiments; Ceara McGowan for histological assistance; Rachel Allison and Olivier Bibari for contributions to implant manufacturing; and Sue Pierce and Joy Parker for animal care. This work was supported by the Colonial Foundation and the Australian National Health and Medical Research Council project grant #1113680. The Bionics Institute acknowledges the support received from the Victorian Government through its Operational Infrastructure Support Program.

6. References

[1] Benabid A L, Pollak P, Gervason C, Hoffmann D, Gao D M, Hommel M, Perret J E and de Rougemont J 1991 Long-term suppression of tremor by chronic stimulation of the ventral intermediate thalamic nucleus *Lancet* **337**(8738) 403-6 Epub 1991/02/16

[2] Rossi P J, et al. 2016 Proceedings of the Third Annual Deep Brain Stimulation Think Tank: A Review of Emerging Issues and Technologies *Front Neurosci* **10** 119 Epub 2016/04/20

[3] Lyons M K 2011 Deep brain stimulation: current and future clinical applications *Mayo Clin Proc* **86**(7) 662-72 Epub 2011/06/08

[4] Foltynie T and Hariz M I 2010 Surgical management of Parkinson's disease *Expert Rev Neurother* **10**(6) 903-14 Epub 2010/06/04

[5] Rowland N C, Sammartino F and Lozano A M 2017 Advances in surgery for movement disorders *Movement Disorders* **32**(1) 5-10

[6] Deuschl G, Paschen S and Witt. K 2013 Clinical outcome of deep brain stimulation for Parkinson's disease *Handbook of Clinical Neurology* Lozano A M, Hallett M: Elsevier) pp 107-28

[7] Rolston J D, Englot D J, Starr P A and Larson P S 2016 An unexpectedly high rate of revisions and removals in deep brain stimulation surgery: analysis of multiple databases *Parkinsonism & related disorders* **33** 72-7

[8] McDermott H 2016 Neurobionics: treatments for disorders of the central nervous system *Neurobionics: the biomedical engineering of neural prostheses Hoboken, NJ: John Wiley & Sons* 213-30

[9] Chan D T, Zhu X L, Yeung J H, Mok V C, Wong E, Lau C, Wong R and Poon W S 2009 Complications of deep brain stimulation: a collective review *Asian J Surg* **32**(4) 258-63 Epub 2009/11/07

[10] Carvallo J F B, Mostile G, Almaguer M, Davidson A, Simpson R and Jankovic J 2012 Deep brain stimulation hardware complications in patients with movement disorders: risk factors and clinical correlations *Stereotact Funct Neurosurg* **90**(5) 300-6

[11] Voges J, Waerzeggers Y, Maarouf M, Lehrke R, Koulousakis A, Lenartz D and Sturm V 2006 Deep-brain stimulation: long-term analysis of complications caused by hardware and surgery--experiences from a single centre *J Neurol Neurosurg Psychiatry* **77**(7) 868-72 Epub 2006/04/01

[12] Morishita T, Okun M S, Burdick A, Jacobson IV C E and Foote K D 2013 Cerebral venous infarction: a potentially avoidable complication of deep brain stimulation surgery *Neuromodulation: Technology at the Neural Interface* **16**(5) 407-13

[13] Ory-Magne F, Brefel-Courbon C, Simonetta-Moreau M, Fabre N, Lotterie J A, Chaynes P, Berry I, Lazorthes Y and Rascol O 2007 Does ageing influence deep brain stimulation outcomes in Parkinson's disease? *Movement disorders: official journal of the Movement Disorder Society* **22**(10) 1457-63

[14] Boviatsis E J, Stavrinou L C, Themistocleous M, Kouyialis A T and Sakas D E 2010 Surgical and hardware complications of deep brain stimulation. A seven-year experience and review of the literature *Acta Neurochirurgica* **152**(12) 2053-62

[15] Dembek T A, et al. 2017 Directional DBS increases side-effect thresholds—A prospective, double-blind trial *Movement Disorders* **32**(10) 1380-8

[16] Schüpbach M, Chabardes S, Matthies C, Pollo C, Steigerwald F, Timmermann L, Visser Vandewalle V, Volkmann J and Schuurman P R 2017 Directional leads for deep brain stimulation: Opportunities and challenges *Movement disorders* **32**(10) 1371-5

[17] Martens H, Toader E, Decré M, Anderson D, Vetter R, Kipke D, Baker K B, Johnson M D and Vitek J L 2011 Spatial steering of deep brain stimulation volumes using a novel lead design *Clinical neurophysiology* **122**(3) 558-66

[18] Fernández-García C, Foffani G, Dileone M, Catalán-Alonso M, González-Hidalgo M, Barcía J and Alonso-Frech F 2017 Directional local field potential recordings for symptom-specific optimization of deep brain stimulation *Movement Disorders* **32**(4) 626-8

[19] Stock G, Sturm V, Schmitt H and Schlör K 1979 The influence of chronic deep brain stimulation on excitability and morphology of the stimulated tissue *Acta neurochirurgica* **47**(1) 123-9

[20] Stypulkowski P H, Giftakis J E and Billstrom T M 2011 Development of a large animal model for investigation of deep brain stimulation for epilepsy *Stereotact Funct Neurosurg* **89**(2) 111-22 Epub 2011/02/22

[21] Awan N R, Lozano A and Hamani C 2009 Deep brain stimulation: current and future perspectives *Neurosurg Focus* **27**(1) E2 Epub 2009/07/03

[22] Bjartmarz H and Rehncrona S 2007 Comparison of accuracy and precision between frame-based and frameless stereotactic navigation for deep brain stimulation electrode implantation *Stereotact Funct Neurosurg* **85**(5) 235-42 Epub 2007/05/31

[23] Zrinzo L 2012 Pitfalls in precision stereotactic surgery *Surg Neurol Int* **3**(Suppl 1) S53-61 Epub 2012/07/25

[24] Petersen E A, Holl E M, Martinez-Torres I, Foltynie T, Limousin P, Hariz M I and Zrinzo L 2010 Minimizing brain shift in stereotactic functional neurosurgery *Neurosurgery* **67**(3 Suppl Operative) ons213-21; discussion ons21 Epub 2010/08/04

[25] Benazzouz A, Breit S, Koudsie A, Pollak P, Krack P and Benabid A L 2002 Intraoperative microrecordings of the subthalamic nucleus in Parkinson's disease *Movement disorders: official journal of the Movement Disorder Society* **17**(S3) S145-S9

[26] Cagnan H, Dolan K, He X, Contarino M F, Schuurman R, van den Munckhof P, Wadman W J, Bour L and Martens H C 2011 Automatic subthalamic nucleus detection from microelectrode recordings based on noise level and neuronal activity *Journal of neural engineering* **8**(4) 046006

[27] Patel N K, Plaha P and Gill S S 2007 Magnetic resonance imaging-directed method for functional neurosurgery using implantable guide tubes *Neurosurgery* **61**(5 Suppl 2) 358-65; discussion 65-6 Epub 2008/01/08

[28] Villalobos J, Fallon J B, McNeill P M, Allison R K, Bibari O, Williams C E and McDermott H J Preclinical evaluation of a miniaturized Deep Brain Stimulation electrode lead *Engineering in Medicine and Biology Society (EMBC), 2015 37th Annual International Conference of the IEEE 2015)*: IEEE

[29] Worrell G A, Gardner A B, Stead S M, Hu S, Goerss S, Cascino G J, Meyer F B, Marsh R and Litt B 2008 High-frequency oscillations in human temporal lobe: simultaneous microwire and clinical macroelectrode recordings *Brain* **131**(Pt 4) 928-37 Epub 2008/02/12

[30] Hefft S, Brandt A, Zwick S, von Elverfeldt D, Mader I, Cordeiro J, Trippel M, Blumberg J and Schulze-Bonhage A 2013 Safety of hybrid electrodes for single-neuron recordings in humans *Neurosurgery* **73**(1) 78-85; discussion Epub 2013/04/26

[31] Connolly A T, et al. 2016 A novel lead design for modulation and sensing of deep brain structures *IEEE Transactions on Biomedical Engineering* **63**(1) 148-57

[32] Berman A L and Jones E G 1982 *The Thalamus and Basal Telencephalon of the Cat: A Cytoarchitectonic Atlas with Stereotaxic Coordinates*: University of Wisconsin Press)

[33] Chen Z J, Gillies G T, Broaddus W C, Prabhu S S, Fillmore H, Mitchell R M, Corwin F D and Fatouros P P 2004 A realistic brain tissue phantom for intraparenchymal infusion studies *J Neurosurg* **101**(2) 314-22 Epub 2004/08/18

[34] Little S and Brown P 2012 What brain signals are suitable for feedback control of deep brain stimulation in Parkinson's disease? *Ann N Y Acad Sci* **1265** 9-24 Epub 2012/07/27

[35] Sinclair N C, McDermott H J, Bulluss K J, Fallon J B, Perera T, Xu S S, Brown P and Thevathasan W 2018 Subthalamic nucleus deep brain stimulation evokes resonant neural activity *Ann Neurol* **83**(5) 1027-31 Epub 2018/05/05

[36] Haberler C, Alesch F, Mazal P R, Pilz P, Jellinger K, Pinter M M, Hainfellner J A and Budka H 2000 No tissue damage by chronic deep brain stimulation in Parkinson's disease *Annals of neurology* **48**(3) 372-6

[37] Nielsen M S, Bjarkam C, Sørensen J, Bojsen-Møller M, Sunde N A and Østergaard K 2007 Chronic subthalamic high-frequency deep brain stimulation in Parkinson's disease–a histopathological study *European journal of neurology* **14**(2) 132-8

[38] Orlowski D, et al. 2017 Brain Tissue Reaction to Deep Brain Stimulation—A Longitudinal Study of DBS in the Goettingen Minipig *Neuromodulation: Technology at the Neural Interface*